Available online at www.sciencedirect.com
SCIENCE DIRECT
Polymer 47 (2006) 1722–1731
polymer
www.elsevier.com/locate/polymer

Ac conductivity and dielectric permittivity of poly(ethylene glycol) during crystallization: Percolation picture

Ingo Alig [a,*], Sergej M. Dudkin [a], Werner Jenninger [a,1], Michał Marzantowicz [b]

[a] *Deutsches Kunststoff-Institut, Schlossgartenstrasse 6, D-64289 Darmstadt, Germany*
[b] *Faculty of Physics, Warsaw University of Technology, Koszykowa 75, 00-662 Warszawa, Poland*

Received 25 April 2005; received in revised form 18 November 2005; accepted 10 December 2005
Available online 20 January 2006

Abstract

Dielectric conductivity and permittivity of poly(ethylene glycol) were measured in the frequency range between 10^1 and 10^6 Hz during non-isothermal crystallization and melting with different cooling/heating rates (5, 10 and 20 K/h). The time development of the conductivity and permittivity spectra during crystallization and melting is discussed in terms of charge carrier diffusion in a percolation network formed by the amorphous phase of the semi-crystalline polymer.

Keywords: Ac conductivity; Dielectric permittivity; Crystallization

1. Introduction

The investigation of semi-crystalline polymers attracted many researchers since more than 40 years (see e.g. [1–6]). Besides its importance for processing of semi-crystalline polymeric materials the issue of polymer crystallization is of large fundamental interest. The morphology as well as the crystallization kinetics and melting behavior have been studied extensively by different techniques, such as light and electron microscopy, X-ray scattering, calorimetry or dielectric spectroscopy [1–10]. The investigations based on dielectric spectroscopy (see e.g. [7–10] and references therein) were focused mainly on the influence of polymer crystallization on the dipolar relaxation. Besides the influence on the molecular dynamics of polymer chains, the formation of crystalline phase is expected to change conductivity and to induce polarization effects.

The occurrence of strong polarization processes above the glass transition temperature can be modeled by polarization on phase boundaries (see p. 87 and 496 in [3]). Assuming that the conductivity of the crystalline phase is considerably lower than the conductivity of the amorphous phase, the increase of dielectric function can be related to interfacial polarization of Maxwell–Wagner–Sillars type caused by trapping of free charges at the boundaries between crystalline structure and amorphous regions. As an additional phenomenon, which is related to changes of the measured conductivity and permittivity of the material, electrode polarization is expected (see p. 91 in [3]). Recently, some authors [9,10] interpreted the changes in the permittivity observed at the early stage of crystallization according to a 'pre-ordered' melt structure model, also proposed by Strobl [11].

In this study we discuss the changes in frequency dependence of the ac conductivity and dielectric permittivity during non-isothermal crystallization and melting of semi-crystalline polymer. The investigations were performed on poly(ethylene glycol) (PEG) with molecular weight of 2000 g/mol, which has relatively fast crystallization kinetics. Since the glass transition temperature of PEG is much lower than the experimental temperature range of this study no frequency dependent contribution from dipole relaxation is expected. Therefore, this system is well suited for study of charge carrier diffusion in the semi-crystalline structure. Research done earlier by one of us [12] has shown, that the frequency dependence of conductivity and permittivity of poly(ethylene oxide) (PEO) is related to coexistence of amorphous and crystalline regions.

In order to get a deeper understanding of the crystallization kinetics and melting and its relation to dielectric properties we performed experiments with well-defined cooling and heating

* Corresponding author. Tel.: +49 6151 16 2404; fax: +49 6151 292855.
E-mail address: ialig@dki.tu-darmstadt.de (I. Alig).
[1] Present address: Bayer Material Science AG, D-51368 Leverkusen, Germany.

0032-3861/$ - see front matter © 2005 Elsevier Ltd. All rights reserved.
doi:10.1016/j.polymer.2005.12.026

rates. As shortly discussed in section 2, there are different approaches to interpret the frequency dependence of complex conductivity in disorders organic systems (see e.g. [13]). However, because semicrystalline polymers build a supermolecular fractal structure (i.e. ion-conductive amorphous regions embedded in an almost non-conducting crystalline structure), use of percolation approach seems to be applicable for the interpretation of changes in the complex conductivity and this concept is tested in present paper.

2. Background

In the framework of the percolation theory a mixture of two materials with different conductivities is modeled by the lattice, constructed of bonds chosen randomly to be a conductor or an insulator [14–17]. The percolation threshold φ_c is defined as a critical value of volume fraction φ of the conductive component, separating two states: (i) for $\varphi<\varphi_c$ only finite clusters of conductor exist and (ii) for $\varphi>\varphi_c$ there are conduction paths between opposite edges of the lattice (infinite cluster). The macroscopic conductivity $\sigma=\sigma'+i\sigma''$ and the permittivity $\varepsilon=\varepsilon'-i\varepsilon''$ of a percolating system have been studied using different physical models. The most common are the equivalent circuit (or intercluster polarization) model [18–26] and the anomalous diffusion model [27–35]. It has been established, both theoretically and experimentally, that near the critical concentration φ_c the dc-conductivity and the static permittivity follow the power laws [18–24]:

$$\sigma_{dc} = \sigma'(\varphi,\omega=0) \propto (\varphi_c-\varphi)^{-s} \quad \varphi<\varphi_c \tag{1}$$

$$\sigma_{dc} = \sigma'(\varphi,\omega=0) \propto (\varphi-\varphi_c)^{t} \quad \varphi>\varphi_c \tag{2}$$

$$\varepsilon_s = \varepsilon'(\varphi,\omega=0) \propto |\varphi-\varphi_c|^{-s'} \quad \varphi<\varphi_c,\ \varphi>\varphi_c \tag{3}$$

where $\omega=2\pi f$ is the angular frequency. The critical exponents s and t were assumed to be universal, i.e. they depend only on the dimension of the percolation system and not on the details of cluster geometry [14,18–24]. The currently accepted values of these exponents [14–17] are: $s=t\approx1.3$ for two-dimensions and $s\approx0.73$, $t\approx2.0$ for three-dimensions. However, some authors (see e.g. [36–38]) have reported experimental values for s and t which disagree with these theoretical values. The frequency dependences of the real part of the conductivity and the real part of the permittivity near the percolation threshold were also predicted to have a power-law form [21–23]:

$$\sigma'(\omega) \propto \omega^{x} \tag{4}$$

$$\varepsilon'(\omega) \propto \omega^{-y} \tag{5}$$

where critical indices x and y should satisfy the relation [22–34]:

$$x+y=1 \tag{6}$$

Eqs. (1)–(5) have general form for both equivalent circuit and anomalous diffusion model. However, there are principal differences between these two models in the way how they explain the behavior of the effective conductivity and the permittivity of the random mixture.

Equivalent circuit model is based on the intercluster polarization picture and does not take into account diffusion inside the clusters. The dielectric exponent s' in Eq. (3) is assumed to be equal to the exponent s, describing the divergent behavior of the conductivity. For the frequency exponents in Eqs. (4) and (5) this model predicts the following relations to the critical exponents s and t [21–23]:

$$x = \frac{t}{s+t} \tag{7}$$

$$y = \frac{s}{s+t} \tag{8}$$

In contrast to this model, in the anomalous diffusion model the capacitances on bonds connecting the different clusters are not taken into account, and the polarization of the medium, within which these clusters are embedded, is taken to be zero. The transport properties of the percolation system are formulated in terms of diffusion (random walk) within the clusters. The linear size of finite clusters is characterized by the correlation length ξ. The correlation length is defined as the mean distance between two sites on the same finite cluster. When φ approaches φ_c, ξ changes as:

$$\xi \propto |\varphi-\varphi_c|^{-\nu} \tag{9}$$

with the same exponent ν below and above the threshold [15,16]. One can interpret ξ as a typical length up to which the cluster is self-similar and can be regarded as a fractal. For the length scales larger than ξ, the structure can be regarded as homogeneous. The correlation time τ_ξ, which a charge carrier needs, on average, to traverse a cluster of correlation length ξ is given by [15,16]:

$$\tau_\xi \propto \xi^{d_w} \propto |\varphi-\varphi_c|^{-\nu d_w} \tag{10}$$

where the exponent d_w is the effective fractal dimensionality of the random walk ('diffusion exponent'). That supposes the existence of the critical frequency:

$$\omega_\xi \propto \frac{1}{\tau_\xi} \propto |\varphi-\varphi_c|^{\nu d_w} \tag{11}$$

For frequencies $\omega<\omega_\xi$ charge carriers can explore different clusters within one period, i.e. the diffusion is normal. For frequencies above ω_ξ the charge carriers visit only parts of the percolation cluster within one period and anomalous diffusion at the fractal percolation clusters takes place. One of the most important results of this model is the expression for the dielectric exponent s' [32,34]:

$$s' = 2\nu-\beta \tag{12}$$

where β is the percolation exponent that characterizes the probability that a site (or a bond) belongs to the infinite cluster (for $\varphi>\varphi_c$). The value s' is a combination of purely geometrical exponents and does not involve the transport exponents s and t. For the frequency exponents in Eqs. (4) and (5) this approach leads to the following relations [32,34]:

Table 1
Currently accepted values of critical exponents

Exponent	Equivalent circuit		Anomalous diffusion	
	$d=2$	$d=3$	$d=2$	$d=3$
t	≈1.3	≈2.0	≈1.3	≈2.0
s	≈1.3	≈0.73	≈1.3	≈0.73
s'	≈1.3	≈0.73	91/36 (≈2.53)	≈1.33
x	0.5	≈0.72	≈0.34	≈0.60
y	0.5	≈0.28	≈0.66	≈0.40

$$x = \frac{t}{\nu(2 + (t-\beta)/\nu)} \tag{13}$$

$$y = \frac{2\nu - \beta}{\nu(2 + (t-\beta)/\nu)} \tag{14}$$

Table 1 summarizes currently accepted values [14–17] for critical exponents in two-($d=2$) and three-($d=3$) dimensions.

It is remarkable that the frequency-temperature-dependence of the complex conductivity σ is similar for variety of quite different disordered materials (see e.g. [39–54]). In all these experiments the real part of the conductivity σ' shows a plateau at low frequencies which bends off at some critical frequency ω_c and results for $\omega \gg \omega_c$ in a power law dependence [3,13]. Jonscher [55] proposed the following equation for the frequency dependence of the real part of the complex conductivity:

$$\sigma'(\omega) = \sigma_0 + A\omega^n = \sigma_0\left[1 + \left(\frac{\omega}{\omega_c}\right)^n\right] \tag{15}$$

with $0 < n \leq 1$. The term $\sigma_0 = \sigma(\omega = 0)$ corresponds to dc conductivity of the system. The exponent n describes the slope of power-law behavior and usually varies between 0.5 and 1.0 [13,41]. It values increases with decreasing temperature and increasing frequency. In good approximation it is possible to assume time–temperature superposition and to scale the normalized conductivity $\sigma'(\omega)/\sigma_0$ with respect to the normalized frequency ω/ω_c (so called 'master curve'). The critical frequency ω_c and the value of dc conductivity σ_0 were found for many disordered materials to fulfill the Barton–Nakajima–Namikawa relation [56]:

$$\sigma_0 = p\Delta\varepsilon\varepsilon_0\omega_c \tag{16}$$

where $\Delta\varepsilon = \varepsilon'(0) - \varepsilon_\infty$, p is a numerical constant of order 1 and $\varepsilon_0 = 8.854 \times 10^{-12}$ F/m is the dielectric permittivity of vacuum. Various models were developed to explain the origin of such 'universality' of ac conductivity in disordered solids. Macroscopic (e.g. 'percolation' model, 'effective medium' approximation) and microscopic (e.g. hopping conduction) approaches were applied. Discussion of these models can be found e.g. in [13]. Although many experimental data on disordered organic solids show such 'universality' some theoretical aspects of this problem are still unclear and no rigorous theory exists.

3. Experimental

PEG was supplied by Merck (Darmstadt, Germany) and used as received. The molar mass of $M_w = 1860$ g/mol and $M_n = 1830$ g/mol was measured by matrix assisted laser desorption/ionization mass spectroscopy (MALDI MS). The equilibrium melting temperature estimated by differential scanning calorimetry (DSC) is $T_m^0 = 324.4$ K. Below this temperature PEG forms crystals, which arrange to a supermolecular spherolitic structure. The final degree of crystallinity of 0.87 was determined by wide angle X-ray scattering (WAXS).

The polymer was melted and poured into a cylindrical glass test-tube. A miniature 10 pF capacitor (trimmer) with 12 parallel-plate gold-coated electrodes was inserted into the melt. The distance between the capacitor plates was 0.4 mm. The test-tube was placed inside of the custom-made cryostat with nitrogen cooling. For temperature control the Novocontrol Quatro Cryosystem was used. The sample was initially heated to 343 K and then cooled to 293 K and heated again up to 343 K. Three series of measurements representing different cooling/heating rate of 5, 10 and 20 K/h were done. The dielectric measurements were performed in a frequency range from 10^1 to 10^6 Hz using an HP 4192A impedance bridge.

The development of the morphology was recorded using a polarization microscope Leitz Orthoplan with a CCD camera (Leica) coupled to a personal computer. Molten sample was poured onto the glass slide and formed a film about 100 μm thick. This film was covered with cover glass. For temperature control a heat stage Mettler Hot Stage 82 with Mettler FP 80 controller was used.

4. Results and discussion

4.1. Conductivity spectra for crystallization and melting

In Fig. 1 real part of the conductivity (σ') measured at 10 Hz, which was the lowest frequency used in our experiment, is plotted versus temperature for cooling/heating cycles with rates of ±5, ±10 and ±20 K/h. These values of conductivity were used as an approximation for the dc conductivity (σ_{dc}).

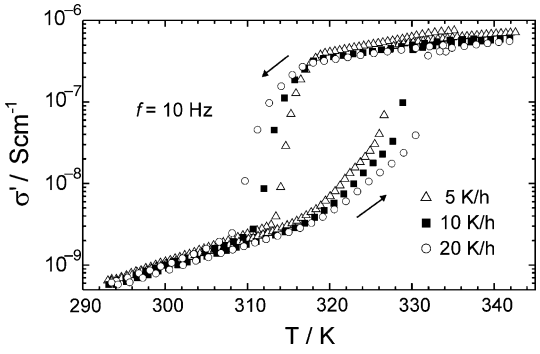

Fig. 1. Temperature dependence of the conductivity for a frequency of 10 Hz for cooling–heating cycles with different heating/cooling rates (indicated in the figure).

The values of the conductivity measured for molten PEG are more than two orders of magnitude higher than for semi-crystalline state. A hysteresis effect between cooling and heating is observed for all cooling/heating rates. The width of the hysteresis loop is decreasing with decreasing cooling/heating rate. In the temperature range below and above the crystallization-melting region similar values of conductivity were obtained independent of cooling rate. The temperature interval for melting is considerable broader than that for crystallization.

Fig. 2 shows frequency dependence of σ' during crystallization for three different cooling rates: 5, 10 and 20 K/h.

For molten polymer σ' is almost independent on frequency. However, for temperatures above 340 K (not shown in Fig. 2), at low frequencies a slight decrease attributed to crossover to frequency region dominated by electrode polarization phenomena was observed, in the discussed temperature range this effect is not present in experimental frequency window and is not expected to influence the spectra of real part of conductivity. For temperatures below 320 K power-law behavior of $\sigma'(f)$ is observed at high frequencies (above about 10^4 Hz) for all cooling rates. As the crystallization continues, four different regions can be distinguished in the conductivity spectra (see e.g. the curve for 309.5 K at 20 K/h in Fig. 2): (i) dc-plateau at low frequencies, (ii) power-low behavior up to about 10^4 Hz, (iii) second 'plateau' up to about 10^5 Hz and (iv) second power-low increase of conductivity

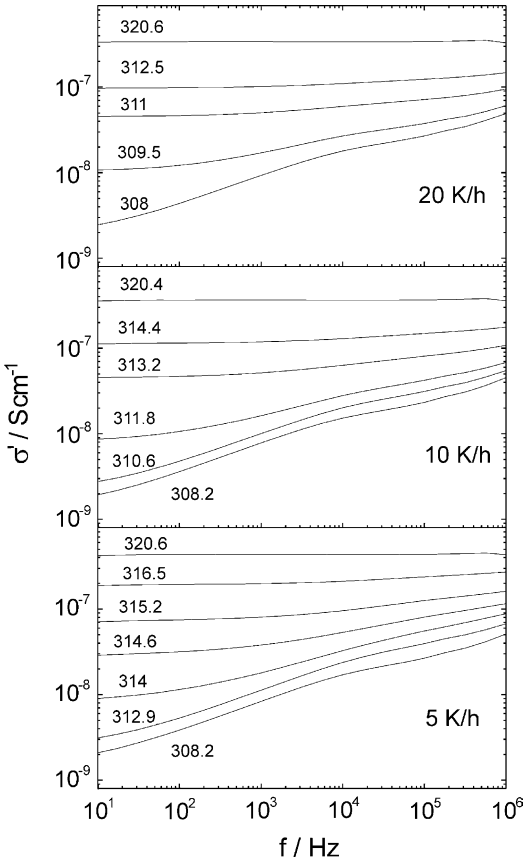

Fig. 2. Frequency dependence of conductivity (σ') during crystallization for different cooling rates (5, 10, 20 K/h). A similar temperature interval, ranging from about 320 to 308 K, is shown for all three experiments.

above about 10^5 Hz. The low-frequency plateau shifts to low frequencies with decreasing temperature and at the final stage of crystallization is moved out of experimental frequency window (i.e. below 10 Hz).

To have an idea which physical processes are responsible for changes in the conductivity spectra below about 10^4 Hz during the process of crystallization described above, we propose a simple model for the morphology–conductivity relationship. The crystallization can be considered as a 'reverse percolation' process (i.e. coming from the high conductivity side). The amorphous phase, forming fractal pathways, is considered to exhibit ionic conductivity, whereas the crystalline phase is assumed to be an insulator. Although the final fraction of the conductive (amorphous) phase in the semi-crystalline PEG might be still higher than the critical (percolation) concentration, the reduction of possible paths for the ion transport is expected to alter the frequency dependence of conductivity and permittivity considerably.

The development of the semi-crystalline structure from the melt is illustrated by a selected sequence of micrographs recorded during cooling of the PEG sample with a rate of about 5 K/h from 343 to 303 K (Fig. 3).

The initial state of the crystallization experiment is an amorphous (melted) polymer, in which nucleation centers are formed (Fig. 3(a)). As the spherulites grow, the amount of amorphous phase decreases. Accordingly the number of possible through-going pathways for the ions goes down, which causes a continuous decrease of dc conductivity. On the next stage of crystallization, the borders of the spherulites partially meet (Fig. 3(b)). At the end of this stage PEG consists of volume filling spherulites, which are composed of lamellae surrounded by confined amorphous material (Fig. 3(c)). However, even when the spherulites borders have merged, the crystallization is not finished. Inside of the spherulites, between the branches of an existing crystalline structure, new lamellae may be formed as observed by Schultz and Miles in an atomic force microscopy study for PEO [57], and the amorphous phase becomes further confined and possibly constrained. It is expected that this effect becomes visible in the conductivity spectra. Melt trapped inside and/or between the spherulites becomes successively the character of a fractal structure. For $\sigma'(f)$ the typical power-law behavior for the ion diffusion in a percolation structure is expected. This power-law behavior is assumed to represent the effective topology of all ion conduction paths within amorphous structures. From the ac conductivity or permittivity data alone we cannot differentiate between more or less constrained amorphous material (e.g. 'rigid amorphous') in the spherulites and/or amorphous material between boundaries of the spherulites (Fig. 3(c)). An explanation for the deviation from the expected high-frequency plateau for frequencies above about 10^5 Hz is the shape of high-frequency power-low dependence of conductivity of amorphous phase itself, as it was found for many disordered materials and discussed in Section 2.

In contrast to the continuous decreasing of conductivity during crystallization, in the melting process two temperature regions with different kinetics can be distinguished (Fig. 1). In the first region conductivity shows only small increase with

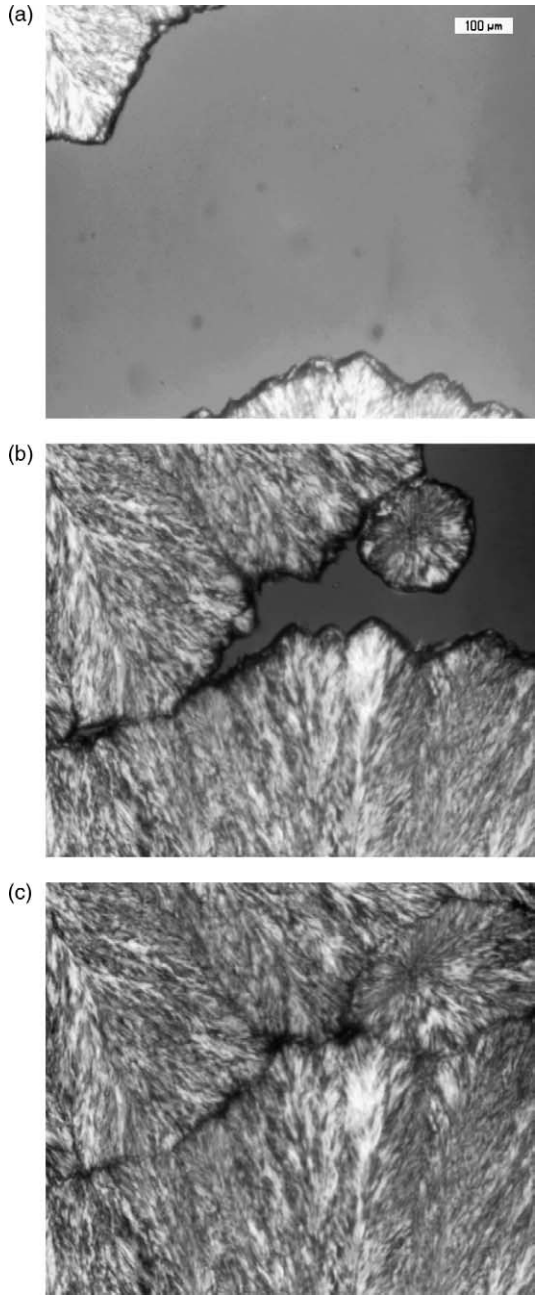

Fig. 3. Polarization micrographs recorded during non-isothermal crystallization of PEG on cooling from 343 to 303 K with a rate of about 5 K/h. The actual temperatures and times after starting the cooling are: (a) 315 K and 332 minutes; (b) 314.5 K and 344 minutes; and (c) 313.1 K and 361 minutes.

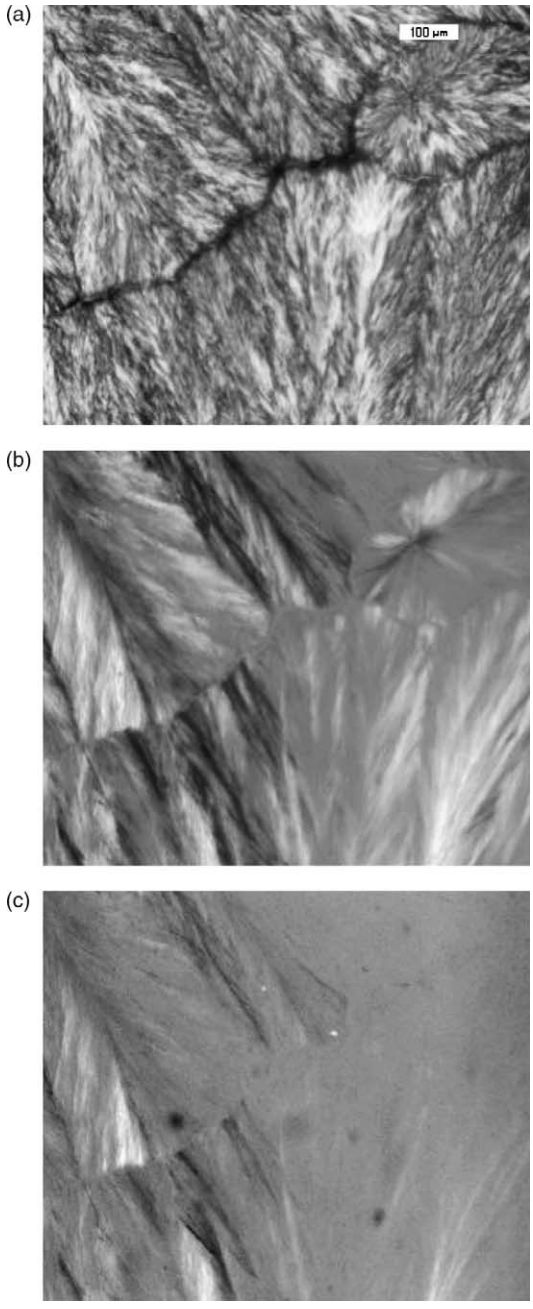

Fig. 4. Polarization micrographs recorded during non-isothermal melting of PEG with a heating rate of about 5 K/h from 303 to 343 K. The actual temperatures and times after starting the heating run are : (a) 312.2 K and 216 minutes; (b) 321.2 K and 216 minutes; and (c) 325.1 K and 261 minutes.

increasing the temperature whereas at the end of the melting conductivity rises rapidly in a very narrow temperature range. The former can be related to the 'softening' and/or melting of less ordered structures in the spherulites, whereas the latter is addressed to the melting of the lamella. The small temperature interval for disappearance of the lamellae can be explained by the well defined melting temperature for a given lamellae thickness. Our assumption is supported by the microscopic pictures shown in Fig. 4 for different stages of melting.

In contrary to the crystallization process, where size and shape of spherulites change, during melting mainly alteration within the spherulite inner morphology was observed (Fig. 4(a) and (b)). At the beginning of the melting, less perfect crystallites probably transform to the melt and the formerly confined amorphous phase gains more freedom of chain movement, e.g. restricted or entangled chains separate from the rigid amorphous phase. This process continues up to some temperature (about 326 K for heating rate 5 K/h) and at the end of this first interval of melting a space-filled spherulitic superstructure build from a 'skeleton' of remaining lamellae is formed (Fig. 4(b) and (c)). A further increase of the temperature by about 0.5 K causes a rapid disappearance of

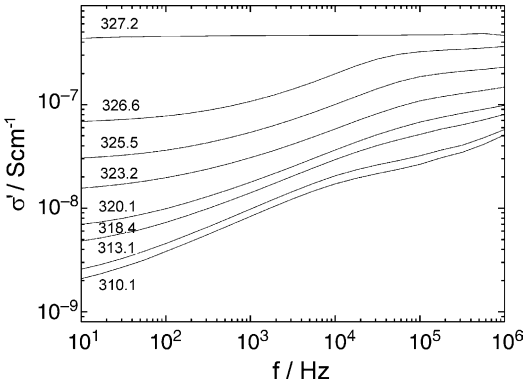

Fig. 5. Conductivity spectra $\sigma'(f)$ recorded at different temperatures during melting with a heating rate of 5 K/h.

the 'skeleton'. Fig. 5 shows the frequency spectra of the conductivity for melting at heating rate of 5 K/h.

As melting starts, the high frequency 'plateau' becomes more pronounced and tends to approach the dc conductivity of the melt. Simultaneously the low frequency conductivity plateau moves gradually into experimental frequency window. At the temperature of about 326 K the conductivity spectrum within the experimental range consists of three regions: two regions with almost constant value of σ' (at low and high frequencies), separated by a region with a power-law behavior of $\sigma'(f)$. Above 326 K only a dc plateau is observed.

From the $\sigma'(f)$ log–log plots, two values which are characteristic for the percolation picture can be derived (Fig. 6): the crossover frequency f_c, at which $\sigma'(f)$ deviates from the dc plateau, and the slope n, representing the exponent of the power-law behavior of $\sigma'(f)$. The values of f_c and n, which seem to be directly related to development (crystallization) or destruction (melting) of crystalline structure, obtained for different temperatures are plotted in Fig. 7.

As mentioned above, at the late stage of crystallization material consist of volume filling spherulites. When an alternating voltage is applied to a material, the charge carriers scan a distance that scales with the period of the electrical field. At low frequencies within one period the ions explore different amorphous regions and the charge carrier diffusion is normal.

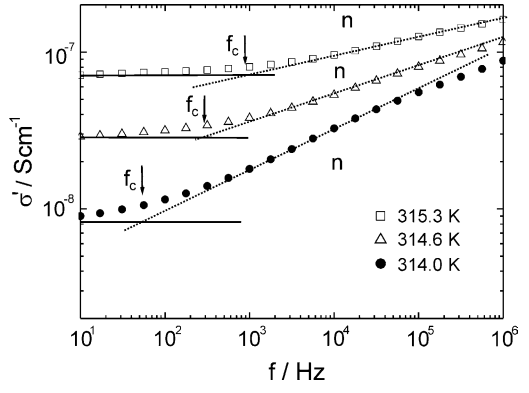

Fig. 6. Analysis of the frequency dependence of ac conductivity: n denotes power law exponent, f_c the crossover frequency. The $\sigma'(f)$ data for three representative temperatures (indicated) are taken from Fig. 2 (cooling rate 5 K/h).

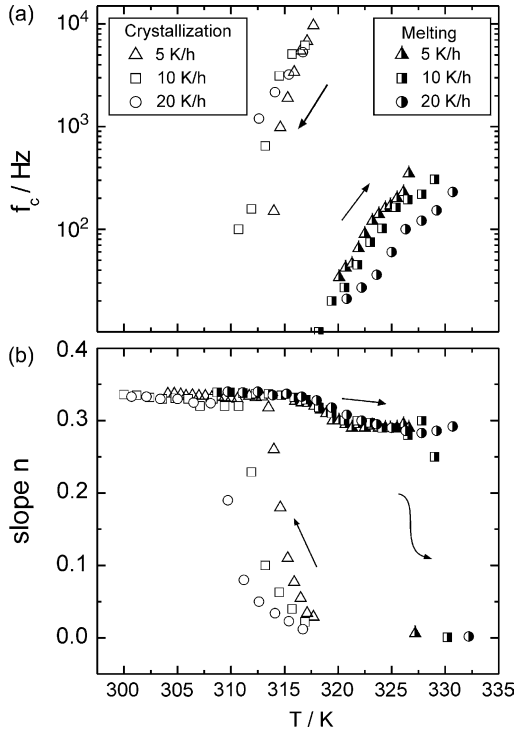

Fig. 7. Temperature dependence of crossover frequency f_c (a) and power law exponent n (b) for non-isothermal crystallization and melting with different cooling rates.

At higher frequencies the ions are expected to travel only within small amorphous areas. Thus we would expect that conductivity approaches the dc value at low frequencies and increase with higher frequencies. From evaluation of parameters σ_{dc} and f_c it was found that, within the investigated range of temperature, the dc conductivity of the sample is proportional to the crossover frequency, fulfilling the Barton–Nakajima–Namikawa relation—Eq. (16). Therefore, it can be assumed, that changes of the microscopic mechanism of conductivity within the amorphous phase due to confinement are not significant in comparison to the discussed changes of conductivity due to 'mesoscopic' topology of the pathways. Diffusion of charge carriers within the small amorphous domains occurs in a similar way as within the free amorphous phase of a molten polymer. The occurrence of high frequency 'plateau' indicates a separation of the microscopic and mesoscopic transport mechanisms. The changes of crossover frequency f_c can be ascribed only to development of the mesoscopic percolation structure. Therefore, it seems to be reasonable to relate the experimental crossover frequency f_c to ω_ξ from Eq. (11). As shown in Fig. 7(a), starting from the temperature of about 318 K, the value of f_c decreases with decreasing temperature, eventually leaving the frequency window of our experiment. According to Eq. (11), this may be related to a 'critical slowing down': $f_c \to 0$ for $\varphi \to \varphi_c$, i.e. the volume fraction of the conductive (amorphous) phase approaches the percolation threshold. In order to replace the temperature (or crystallization time) by the actual content of the amorphous phase, we performed calorimetric experiments (DSC) with identical cooling rates. However, due to the

different thermal conditions in the DSC pans and the dielectric cell the crystallization kinetics were different and the rescaling of the temperature in Fig. 7 with the content at the amorphous phase was not reliable. For such a rescaling DSC or X-ray scattering experiments in situ with dielectric spectroscopy are needed.

The exponent n (slope of $\sigma'(f)$ on a log–log scale) rises as the crystallization proceeds and approaches an almost constant value of 0.34 for the final stage of crystallization (Fig. 7(b)). This behavior is similar for all cooling rates. Again, one should assume that the observed changes are mainly of mesoscopic origin. The onset of power law dependence of conductivity related to intrinsic disorder of the amorphous phase may influence the slope value at the beginning of crystallization, but at later stage the two phenomena become clearly separated. Taking into account the final content of the amorphous phase of 13% (obtained from WAXS) and the tremendous decrease of f_c during crystallization, we assume that our system is not far from the percolation threshold. The value of 0.34 is close to the value of the exponent x in Eq. (4), predicted from the anomalous diffusion model in two dimensions, and lower than the predicted values of x in three dimensions for both equivalent circuit and anomalous diffusion models (Table 1). This may be explained by epitactic growth of the spherulites at the plates of a capacitor, which is known to result in deformed spherulites with lamellae and amorphous regions oriented perpendicular to the plates [58]. Alternatively, for the assumption of three-dimensional percolation the concentration of the conducting amorphous phase would be clearly above the critical concentration φ_c.

During the melting the value of f_c increases with increasing temperature, however, these changes are less pronounced than the changes in f_c during the crystallization. Again, according to Eq. (11), increase in f_c for the melting may indicate an increase of the amount of the conductive fraction with respect to the critical concentration φ_c. Since the spherulitic structure still remains (see micrographs in Fig. 4), this can only be related to melting and/or rearrangements inside the spherulites. The changes in the conductivity spectra are well visualized in the master plot shown in Fig. 8 for $\sigma'(f)$ curves recorded during heating with a rate of 5 K/h. It is clearly seen that in the first phase of melting the frequency range where $\sigma'(f)$ shows power-law behavior becomes narrower with increasing temperature. This can be an indication that the structure gets simpler (less branched). The decreasing difference between conductivity values corresponding to low frequency (dc) plateau and high frequency plateau, which occurs on heating is related to increasing fraction of amorphous phase. As shown in Fig. 7, with increasing heating rate f_c shifts to higher temperatures, however, similar type of f_c vs. T dependence is observed for all heating rates.

As presented in Fig. 7(b), the exponent n shows only a slight decrease from the initial value of about 0.34 with increasing in temperature. In Fig. 8, in the frequency range below the onset of high frequency 'plateau', all presented curves overlay. The dc conductivity σ_{dc} is proportional to f_c and fulfills the BNN relationship (Eq. (16)). This indicates that despite of the increase of the volume fraction of amorphous material, the fractal dimension of the charge carrier diffusions and the mechanism of ion diffusion are almost unchanged. This can be explained by the remaining supermolecular structure of the crystalline frame 'skeleton'. In contrast to the gradual changes of f_c and in the conductivity spectra in the initial phase of melting, in the last stage all features of the frequency dependence of σ' related to crystalline structure disappear abruptly: after melting only a dc plateau, representing ion conductivity in the amorphous phase is observed.

4.2. Permittivity spectra for crystallization and melting

Fig. 9 presents the spectra of the real part of permittivity (ε') for different temperatures in the interval from 320 to 308 K for a non-isothermal crystallization experiment with a cooling rate of 5 K/h.

At low frequencies a tremendous decrease of the permittivity with proceeding crystallization is recorded, whereas in the middle frequency region an initial increase is found which is followed by a decrease at the late stage of crystallization. At high frequencies the permittivity decreases again with proceeding crystallization. A similar change of spectral

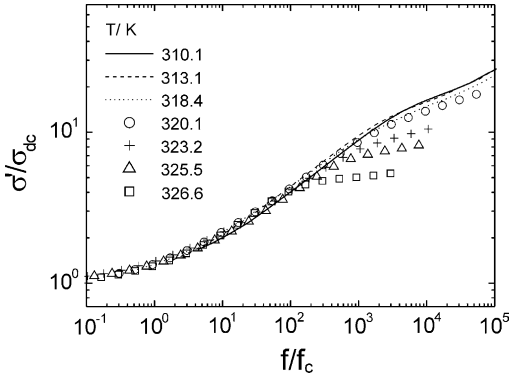

Fig. 8. Reduced plot of the conductivity data measured for melting at 5 K/h heating rate. Scaling variables are f_c and σ_{dc}.

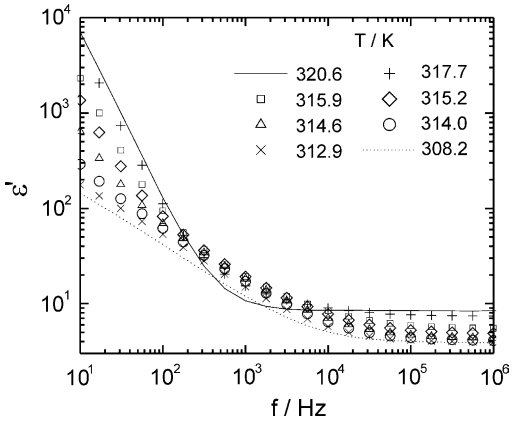

Fig. 9. Frequency dependence of the real part of dielectric permittivity (ε') for different temperatures during crystallization with a cooling rate of 5 K/h.

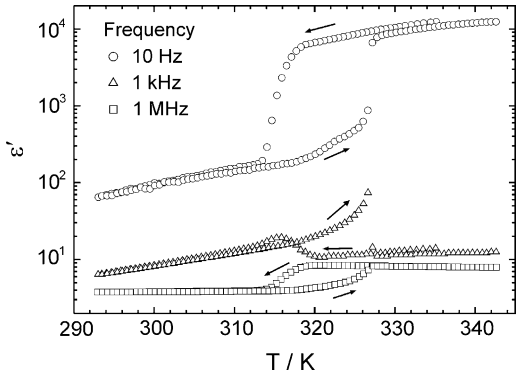

Fig. 10. Temperature dependence of real part of the dielectric permittivity (ε') for representative frequencies (indicated) recorded during cooling-heating cycles (cooling/heating rate 5 K/h).

dependence of ε' during crystallization was recently reported for PCL [9].

The temperature dependence of the real part of the complex permittivity for 10 Hz, 1 kHz and 1 MHz is plotted in Fig. 10 as a function of temperature for crystallization-melting cycle with a cooling/heating rate of 5 K/h. The three frequencies are chosen to represent frequency intervals with different temperature dependence of ε', which are related to different polarization mechanisms.

For low frequencies (10 Hz in Fig. 10) mainly electrode polarization, taking place at polymer/electrode interface, is responsible for the observed changes. The shape of hysteresis curve observed for ε' at low frequencies for crystallization and melting is similar to that in the dc conductivity plot (Fig. 1). The continuous decrease in ε' during crystallization can be explained by decrease in charge carrier mobility, e.g. trapping of the charge carriers in the crystallites or at the crystalline/amorphous interfaces, resulting in the reduction of number of ions which can reach electrodes. Another reason for the decrease of the permittivity during the crystallization could be the reduction of the contact area of semi-crystalline polymer with the electrode in comparison to the melt. During heating a slight increase of the low frequency value of permittivity is observed up to 326 K, which indicates the release of trapped charge carriers. This is in agreement to the transformation of less perfect crystallites and/or rigid amorphous phase to the amorphous melt as discussed above. At the final state of melting (destruction of the 'skeleton') a sharp rise of ε' is observed. This can be explained by the release of ions trapped inside the lamellae and those located at the crystalline/amorphous surface. However, one should take into account that there is another factor which influences the shape of curve in Fig. 10: the frequency range at which electrode phenomena have dominant contribution to the permittivity spectra shifts with rising conductivity.

At high frequencies (1 MHz in Fig. 10) mainly the dipole polarization is expected to contribute to the real part of the permittivity [59]. As already mentioned, the temperature range for crystallization and melting processes is much above the range in which dispersion of ε' related to dipolar relaxations of polymer chain could be observed in the experimental frequency window. For molten polymer ε' rises when the temperature decreases, as expected (see e.g. p. 448 in [3]). When crystallization takes place, the local rearrangements of polymer chains become constrained by the crystalline phase. Consequently the dipole relaxation strength ($\Delta\varepsilon$) decreases which results in lowering of the value of ε'. During the melting the high frequency value of the permittivity increases gradually. This correlates with a gradual change of spherulite color in the polarizing microscope observations, since refraction index of the observed medium is directly coupled with the high frequency limiting value of the permittivity.

In the middle frequency region (1 kHz in Fig. 10) changes in the dielectric function during crystallization and melting can be interpreted in terms of Maxwell–Wagner–Sillars polarization on internal surfaces [60]. Following this model the rise in the real part of permittivity during crystallization (cooling from 320 to 316 K in Fig. 10) can be explained by the growth of the crystalline phase (lamellae and spherulites) and charge polarization on the boundaries of crystalline or rigid amorphous phase. At the maximum the polarization effect due to creation of internal surfaces is compensated by the reduction of free charge carriers due to crystallization. A similar dependence of ε' for middle frequencies was also observed for crystallization of PCL [9], however, the authors have related it to 'pre-ordering' of polymer before crystallization. The situation for melting is somehow different. In the first interval of melting (heating up to 326 K for 5 K/h heating rate) a slight increase in ε' can be seen in Fig. 10, which gets more pronounced with increasing temperature. This rise of permittivity is expected to be mainly caused by the increase of the ion conductivity due to the melting of less perfect crystallites and/or the transformation of rigid amorphous material to the melt, which increases the polarization on the crystal/amorphous interfaces. This is supported by fact, that the 'skeleton' formed by the lamellae is remaining up to the last stage of melting which guaranties a sufficient internal surface for Maxwell–Wagner–Sillars-type polarization. At the last stage of melting (at about 327 K) a sharp drop of ε' of about one order of magnitude is observed. This is a point at which a rapid melting of remaining crystalline lamellae ('skeleton') takes place and the internal surfaces for polarization disappear completely.

An explanation alternative to the Maxwell–Wagner–Sillars approach can be given in the frame of charge carrier diffusion model. Development of heterogeneous structure leads to tremendous increase of permittivity with approaching the percolation threshold (Eq. (3)). Therefore, the features in both models are similar. The time needed to explore the percolation structure by the charge carriers is equivalent to the time necessary to transfer charges to the microcapacitors formed by the semi-crystalline structure. The increase of ε' during crystallization (cooling from 320 to 316 K) in Fig. 10 can be explained by approaching the percolation threshold, i.e. the formation of a percolation network of the conducting amorphous phase by the growth of crystalline structures. As the crystallization continues the creation of the fractal percolation network is compensated by the decrease of the

number of free charge carrier trapped in the crystalline phase. The initial rise of permittivity during melting can therefore, be explained by the release of the trapped ions, while crystalline 'skeleton' is only gradually changing. The tremendous decrease of the middle frequency value of the permittivity at about 327 K is caused by a complete destruction of the semicrystalline percolation structure.

5. Conclusions

In this paper, we have presented frequency dependent measurements of the ac conductivity and permittivity for poly(ethylene glycol) during non-isothermal crystallization and melting with different cooling/heating rates. A simple percolation model for the semi-crystalline polymer structure during crystallization and melting was proposed. The morphology data obtained from polarization microscopy were used to support this model.

The main conclusions can be summarized as follows:

(1) The analysis in the frame of percolation model shows, that during crystallization a percolation network for ion transport is formed by the remaining amorphous phase. The ion-conducting network in semi-crystalline polymer was found to be close to percolation threshold, but most probably still above it.
(2) The analysis of the conductivity as well as of the permittivity spectra shows an asymmetry between crystallization and melting. The gradual changes in charge transport and polarization during crystallization can be explained by nucleation and continuous growth of lamellae and spherulites. For the melting we identified two stages: (i) melting and rearrangements of less ordered structures and/or rearrangements of restricted amorphous material (e.g. 'rigid amorphous phase') in the spherulites over a broad temperature range and (ii) the melting of the lamellae of the spherulitic superstructure ('skeleton') in a very small temperature interval.

These conclusions are in agreement with our recent paper [61] where we analyzed the same experimental data in the frame of equivalent circuit model. The results presented here show clearly that dielectric spectroscopy is a viable method for determination of the morphological changes of semi-crystalline polymers in the process of crystallization or melting. To get an additional support for our assumption of the percolation nature of observed phenomena, we will perform isothermal crystallization experiments. To replace time or temperature by the actual fraction of the amorphous phase, the degree of crystallinity should be measured under identical conditions with an independent method (e.g. X-ray scattering, calorimetry, light scattering or ultrasound). Although we think that the percolation approach can explain the main features of the crystallization in polymers, we are aware that for better understanding of the conductivity and permittivity spectra of semicrystalline polymers other effects (such as electrode polarization, surface polarization on crystallites, ion-conductivity in the disordered amorphous phase) should be analyzed more detailed by combining different concepts.

Acknowledgements

The authors would like to thank for support from the Forschungsgesellschaft Kunststoffe e.V., the Fond der Chemischen Industrie, the European Science Foundation and the Center of Photonics and Materials for Prospective Applications (CEPHOMA).

References

[1] McCrum NG, Read BE, Williams G. Anelastic and dielectric effects in polymeric solids. Wiley: New York; 1967.
[2] Runt JP, Fitzgerald JJ. Dielectric spectroscopy of polymer materials. Washington, DC: American Chemical Society; 1997.
[3] Kremer F, Schönhals A. Broadband dielectric spectroscopy. Heidelberg: Springer; 2002.
[4] Mandelkern L. Crystallization of polymers. New York: McGraw Hill; 1964 [see also 2nd ed, vol. 1. Cambridge: Cambridge University Press; 2002].
[5] Wunderlich B. Macromolecular physics, vols. I–III. New York: Academic Press; 1976.
[6] Schultz JM. Polymer crystallization. Oxford: Oxford University; 2000.
[7] Ezquerra TA, Majszczyk J, Balta-Calleja FJ, Lopez-Cabaros E, Gardner KH, Hsiao BS. Phys Rev B 1994;9(50):6023–31.
[8] Ezquerra TA, Liu F, Boyd RH, Hsiao BS. Polymer 1977;38:5793–800.
[9] Wurm A, Soliman R, Schick C. Polymer 2003;44:7467–76.
[10] Fukao K, Miyamoto Y. Phys Rev Lett 1997;79(23):4613–6.
[11] Strobl G. Eur Phys J E 2000;3:165–83.
[12] Dygas JR, Misztal-Faraj B, Florjańczyk Z, Krok F, Marzantowicz M, Zygadło-Monikowska E. Solid State Ionics 2003;157:249–56.
[13] Dyre JC, Schroeder TB. Rev Mod Phys 2000;72(3):873–92.
[14] Clerc JP, Giraud G, Laugier JM, Luck JM. Adv Phys 1990;39(3): 191–309.
[15] Bunde A, Havlin S. Fractals and disordered systems. Berlin: Springer; 1996.
[16] Stauffer D, Aharony A. Introduction to percolation theory. London: Taylor & Francis; 1994.
[17] Sahimi M. Applications of percolation theory. London: Taylor & Francis; 1994.
[18] Kirkpatrick S. Rev Mod Phys 1973;45:574–88.
[19] De Gennes PG. J Phys Lett (Paris) 1976;37:L1.
[20] Efros AL, Shklovskii BI. Phys Status Solidi B 1976;76:475–85.
[21] Straley JP. J Phys C: Solid State Phys 1976;9:783–95.
[22] Bergman DJ, Imry Y. Phys Rev Lett 1977;39(19):1222–5.
[23] Webman I, Jortner J, Cohen MH. Phys Rev B 1977;16(6):2593–6.
[24] Stephen MJ. Phys Rev B 1978;17(11):4444–53.
[25] Stroud D, Bergman DJ. Phys Rev B 1982;25(3):2061–4.
[26] Wilkinson D, Langer JS, Sen PN. Phys Rev B 1983;28(2):1081–7.
[27] Scher H, Lax M. Phys Rev B 1973;7(10):4491–519.
[28] De Gennes PG. La Recherche 1976;7:919.
[29] Stauffer D. Phys Rep 1979;54(1):1–74.
[30] Straley JP. J Phys C: Solid State Phys 1980;13:2991–3002.
[31] Gefen Y, Aharony A, Mandelbrot BB, Kirkpatrick S. Phys Rev Lett 1981; 47(25):1771–4.
[32] Gefen Y, Aharony A, Alexander S. Phys Rev Lett 1983;50(1):77–80.
[33] Weiss GH, Rubin RJ. Adv Chem Phys 1983;52:363–505.
[34] Laibowitz RB, Gefen Y. Phys Rev Lett 1984;53(4):380–3.
[35] Hong DC, Stanley HE, Coniglio A, Bunde A. Phys Rev B 1986;33(7): 4564–73.
[36] Reghu M, Yoon CO, Yang CY, Moses D, Smith P, Heeger AJ, et al. Phys Rev B 1994;50(19):13931–41.
[37] Wu J, McLachlan DS. Phys Rev B 1998;58(22):14880–7.

[38] Fraysse J, Planès J. Phys Stat Solid B 2000;218:273–7.
[39] Kremer F, Dominguez L, Meyer WH, Wegner G. Polymer 1989;30(11): 2023–9.
[40] Roling B, Happe A, Funke K, Ingram MD. Phys Rev Lett 1997;78(11): 2160–3.
[41] Sidebottom DL. Phys Rev Lett 1999;83(5):983–6.
[42] Bunde A, Maass P. J Non-Cryst Solids 1991;131/133(2):1022–7.
[43] Rozanski SA, Kremer F, Köberle P, Laschewsky A. Macromol Chem Phys 1995;196(3):877–90.
[44] Ahlskog M, Reghu M, Heeger AJ. J Phys: Condens Matter 1997;9(20): 4145–56.
[45] Capaccioli S, Lucchesi M, Rolla PA, Ruggeri G. J Phys: Condens Matter 1998;10:5595–617.
[46] Tajitsu T. J Mater Sci Lett 2001;20:1159–62.
[47] Ratner MA, Nitzan A. Faraday Discuss Chem Soc 1989;88:19–42.
[48] Dutta P, Biswas S, De KS. J Phys: Condens Matter 2001;13(41): 9187–96.
[49] McLachlan DS, Heaney MB. Phys Rev B 1999;60(18):12746–51.
[50] Chakrabarty RK, Bardhan KK, Basu A. J Phys: Condens Matter 1993;5: 2377–88.
[51] Adriaanse LJ, Reedijk JA, Teunissen PAA, Brom HB, Michels MAJ, Brokken-Zijp JCM. Phys Rev Lett 1997;78(9):1755–8.
[52] Connor MT, Roy S, Ezquerra TA, Balta Calleja FJ. Phys Rev B 1998; 57(4):2286–94.
[53] Jäger K-M, McQueen DH, Tchmutin IA, Ryvkina NG, Klüppel M. J Phys D: Appl Phys 2001;34:2699–707.
[54] Pötschke P, Dudkin SM, Alig I. Polymer 2003;44:5023–30.
[55] Jonscher AK. Nature 1977;267:673–9.
[56] Namikawa H. J Non-Cryst Solids 1975;18:173–95.
[57] Schultz JM, Miles MJ. J Polym Sci, Part B: Polym Phys 1998;36: 2311–25.
[58] Ton-That TM, Jungnickel BJ. J Appl Polym Sci 1999;74:3275–85.
[59] Porter CH, Boyd RH. Macromolecules 1971;4:589–94.
[60] Sillars RW. J Inst Electr Eng 1937;80:378–94.
[61] Marzantowicz M, Dygas JR, Jenninger W, Alig I. Solid State Ionics 2005; 176:2115–21.